scientific reports

Check for updates

OPEN

Role of Cattaneo–Christov heat flux in an MHD Micropolar dusty nanofluid flow with zero mass flux condition

Muhammad Ramzan[1]✉, Hina Gul[1], Dumitru Baleanu[2,3,4], Kottakkaran Sooppy Nisar[5] & M. Y. Malik[6]

This investigation aims to look at the thermal conductivity of dusty Micropolar nanoliquid with MHD and Cattaneo–Christov heat flux flow over an elongated sheet. The novelty of the envisioned mathematical model is augmented with the added impacts of the heat source/sink, chemical reaction with slip, convective heat, and zero mass flux boundary conditions. The salient feature of the existing problem is to discuss the whole scenario with liquid and dust phases. The graphical depiction is attained for arising pertinent parameters by using bvp4c a built-in MATLAB function. It is noticed that the thermal profile and velocity field increases for greater values of liquid particle interaction parameter in the case of the dust phase. An escalation in the thermal profile of both liquid and dust phases is noticed for the magnetic parameter. The rate of mass transfer amplifies for large estimates of the Schmidt number. The thickness of the boundary layer and the fluid velocity are decreased as the velocity slip parameter is augmented. In both dust and liquid phases, the thermal boundary layer thickness is lessened for growing estimates of thermal relaxation time. The attained results are verified when compared with a published result.

List of symbols

B_0	Magnetic field strength
$k*$	Rotational coefficient
ρ_j	Density of micro-inertia
τ_m	Velocity relaxation time
C	Concentration of the fluid
C_w	Concentration of nanoparticles
C_∞	Free stream concentration of nanoparticles
N_t	Thermophoresis parameter
Pr	Prandtl number
c_p	Specific heat
c_s	Specific heat of dust particles
K_r	Chemical reaction
x, y	Coordinate axis
D_B	Brownian diffusion coefficient
E	Angular velocity
Re_x	Local Reynold number
T	Temperature of fluid
q_n	Mass flux
τ_c	Mass relaxation of a dust particle
h_f	Heat transfer coefficient

[1]Department of Computer Science, Bahria University, Islamabad 44000, Pakistan. [2]Department of Mathematics, Cankaya University, 06790 Ankara, Turkey. [3]Institute of Space Sciences, 077125 Magurele-Bucharest, Romania. [4]Department of Medical Research, China Medical University Hospital, China Medical University, Taichung 40447, Taiwan. [5]Department of Mathematics, College of Arts and Sciences, Prince Sattam Bin Abdulaziz University, Wadi Aldawaser 11991, Saudi Arabia. [6]Department of Mathematics, College of Sciences, King Khalid University, Abha 61413, Saudi Arabia. ✉email: mramzan@bahria.edu.pk

B_1	Biot number
T_p	Dust particles temperature
ρ_p	Density of dust particle
C_p	Dust particles concentration
$\alpha*$	Slip coefficients
M	Magnetic parameter
D_p	Ration of density of nanofluid to the density of dust particles
$G*$	Micropolar material parameter
τ_w	Shear stress
Sh_x	Sherwood number
δ	Slip parameter
k	Thermal conductivity
ε	Viscosity of spin gradient
ρ_p	Density of dust particles
σ	Electrical conductivity of liquid
q_n	Mass flux
l	Characteristic length
m	Mass of dust particles
λ_1	Thermal relaxation time coefficient
N_b	Brownian motion parameter
T_∞	Ambient temperature
u, v	Components of velocity
u_p, v_p	Velocity of dust particles
Q	Source/sink parameter
η	Similarity variable
D_T	Thermophoresis diffusion coefficient
ν	Kinematic viscosity
ρ	Density of fluid
τ	Ratio of nanoparticles
T_p	Temperature of a dust particle
τ_T	Relaxation time of the dust particle
Γ	Specific heat ratio of the mixture
u_e	Stretching velocity
τ	Ratio of specific heat
b	Constant
μ	Dynamic viscosity
B	Coupling constant parameter
λ	Ratio of viscosity of spin gradient to the density of particle phase
γ	Thermal relaxation parameter
C_F	Skin friction
α_d	Fluid particle interaction parameter

Nanofluid is a combination of nanometer-sized particles and a base fluid that helps to improve the heat capacity of the solution. The addition of millimeter or micrometer small particles (dust particles) to base fluids improves thermal conductivity and is referred to as Dusty fluid. The influence of Micropolar dust particles with MHD in a non-Darcy porous system is observed by Hady et al.[1]. It is witnessed in this analysis that the velocity magnitude for both dust and fluid phases boosts for variable concentration. It is also noticed that the temperature upsurges for the Darcy number and convective parameter. Begum et al.[2] analyzed numerically the Dusty nanoliquid of gyrotactic microorganisms along a vertical isothermal surface. Nabwey and Mahdy[3] investigated dusty particles with a nonlinear temperature of Micropolar natural convection nanoliquid flow past a permeable cone. It is discovered from the results that increasing the suction variable boosts the local Nusselt number. Nabwey and Mahdy[4] in another study examined unsteady non-Newtonian hybrid nanoliquid flow filled with Fe_3O_4–Ag dust nanoparticles over a stretched surface under the influence of MHD free convection with surface temperature and a prescribed heat flux of boundary conditions. The numerical solution of the problem is acquired using a Finite Difference Method. Some recent studies highlighting nanoliquid flow may be found in[5–23] and many therein.

Owing to enormous applications in nanofluid mechanics, researchers are working on the heat transfer mechanism in the form of a wave instead diffusion process[24–26]. It is a understood phenomenon that the transfer of heat occurs owing to temperature differences amongst two different objects or within the components of the same system. The basic heat conduction law coined by Fourier[27] has been a yardstick for decades to gauge the heat transfer characteristics. Later, it was noticed with concern that this model ends up with a parabolic energy equation that experiences a disturbance at an initial stage that lasts throughout the process. This drawback in the Fourier model is signified as a "paradox of heat conduction". This shortcoming is addressed by Cattaneo[28] by introducing the relaxation term in the Fourier model. Later, Christov[29] established the relation suggested by Cattaneo through frame-indifferent change with the Oldroyd upper-convected derivative. Such association is labeled as Cattaneo–Christov (CC) flux model. Kumar et al.[30] researched the characteristics of Dusty fluid of suspended hybrid nanoparticles flows in two phases over an extended cylinder with a CC flux model. For numerical results, the fourth fifth Runge–Kutta–Fehlberg order system was used, as well as the shooting methodology. It is noticed that the thermal profile and thickness of the thermal boundary layer are higher for the relaxation time

	Dusty fluid	Nanofluid flow	Velocity slip	Zero mass flux	Cattaneo Christov heat flux	Micropolar fluid	Chemical reaction	Convective boundary
Hady et al.[1]	Yes	No	No	No	No	Yes	No	Yes
Gireesha et al.[35]	Yes	No	No	No	Yes	No	No	No
Begum et al.[2]	Yes	Yes	No	No	No	No	No	No
Souayeh et al.[36]	Yes	Yes	Yes	No	No	No	No	No
Anuar et al.[37]	Yes	Yes	Yes	No	No	No	No	No
Present work	Yes	Yes	Yes	Yes	Yes	Yes	Yes	Yes

Table 1. Assessment of the present work with the close related published works.

parameter due to the melting effect. Ramzan et al.[31] analyzed the Williamson fluid flow numerically with the CC flux model and magnetohydrodynamic effect with heterogeneous reactions near a stagnation point. It is noted that the Williamson fluid parameter has an opposing effect on temperature and velocity profiles. Prasad et al.[32] conducted an analytical study of Williamson nanofluid flow with the Cattaneo–Christov theory using variable thickness. Heat transfer examination of non-Newtonian nanoliquid flow with convective boundary conditions and CC flux model over an oscillatory surface is assessed analytically by Ullah et al.[33]. It is examined that the liquid velocity is suppressed for Hartmann and Deborah numbers.

The aforementioned studies disclose that plenty of explorations may be quoted on the subject of nanofluid flows. Nevertheless, fewer researches are pondered in the literature that signify the nanofluid flow with dust particles amalgamation. But no study is discussed so far in the literature that pondered the Cattaneo–Christov heat flux on an MHD Micropolar dusty nanofluid flow over a stretched surface with slip, convective heat, and zero mass flux conditions. The originality of the modeled problem is augmented with the additional impacts of the chemical reaction and heat source/sink. Thus, the association of dust particles, Micropolar nanofluid, and slip, convective, and zero mass flux condition boundary conditions is supposed to present a remarkable problem in liquid dynamics based on these physical assumptions. To portray a clear picture of the uniqueness of the present analysis Table 1 is erected by comparing it with the associated published works.

The prime objective of the presented model is to answer the subsequent answers:

1. How fluid velocity and temperature are affected by fluid-particle interaction effects?
2. How dust and fluid phases for velocity and temperature profiles are influenced by the magnetic parameter?
3. What is the association of the thermal relaxation parameter with the fluid velocity and the temperature in case of both phases?
4. How fluid velocity is influenced by the slip parameter?
5. What is the impact of the chemical reaction on the rate of the mass transfer?
6. How fluid temperature is affected by the heat source/sink for both liquid and dust phases?

Mathematical model

The dusty Micropolar, incompressible, steady, MHD nanofluid flow is assumed over an extending sheet with restriction $y > 0$, and we have considered two forces acting along y- and x-direction respectively. where the y-axis is considered to be normal in the flow direction. B_0 is the magnetic field. The outline of the proposed mathematical model is given in Fig. 1.

Following Oberbeck-Boussinesq, the boundary layer approximation, and the notion that the dust particles have the same size and their density remains constant throughout the fluid flow, the governing system of equations for the fluid phase and the dust particles is given in the subsequent set of equations:

The Fluid Phase[1,35].

$$u_x + v_y = 0, \tag{1}$$

$$uu_x + vu_y = \nu u_{yy} + \frac{k^*}{\rho}E_y - \frac{\sigma B_0^2}{\rho}u + \frac{\rho_p}{\rho\tau_m}(u_p - u), \tag{2}$$

$$uE_x + vE_y = \frac{\varepsilon}{\rho_j}E_{yy} - \frac{k^*}{\rho_j}(2E + u_y), \tag{3}$$

$$\begin{aligned} &uT_x + vT_y + \lambda_1\left[u^2T_{xx} + v^2T_{yy} + 2uvT_{xy} + (uu_x + vu_y)T_x + (uv_x + vv_y)T_y\right] \\ &= \alpha T_{yy} + \frac{\rho_p c_s}{\tau_T}(T_p - T) + \frac{Q_0}{\rho c_p}(T - T_\infty) + \tau D_B C_y T_y + \frac{\tau D_T}{T_\infty}T_y^2, \end{aligned} \tag{4}$$

$$uC_x + vC_y = D_B C_{yy} + \frac{D_T}{T_\infty}T_{yy} - K_r(C - C_\infty) + \frac{m\rho_p}{\rho\tau_c}(C_p - C). \tag{5}$$

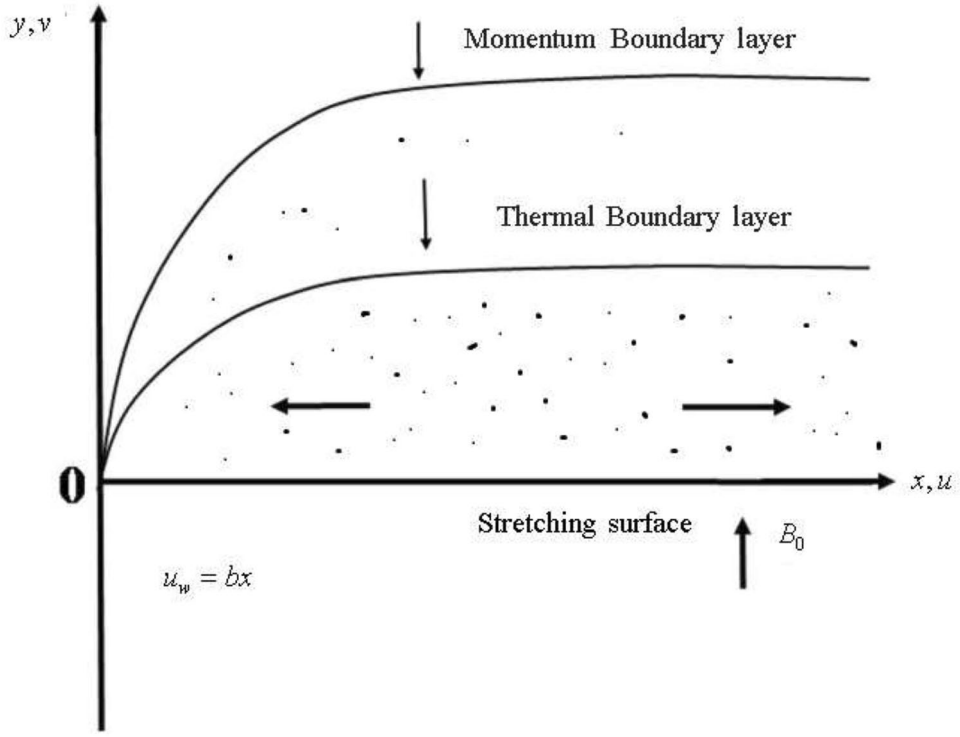

Figure 1. Flow illustration.

The dust phase.

$$u_{px} + v_{py} = 0, \tag{6}$$

$$u_p u_{p_x} + v_p u_{p_y} = -\frac{1}{\tau_m}(u_p - u), \tag{7}$$

$$\rho_p c_s \left(u_p T_{p_x} + v_p T_{p_y}\right) = \frac{-\rho_p c_s}{\tau_T}(T_p - T), \tag{8}$$

$$u_p C_{px} + v_p C_{py} = \frac{-m\rho_p}{\rho\tau_c}(C_p - C). \tag{9}$$

The correlated boundary conditions are presented as below:

$$\begin{aligned} &u = bx + \alpha^* u_y,\ v = 0,\ E = -n_1 u_y,\ -kT_y = h_f(T_f - T),\ D_B C_y + \frac{D_T}{T_\infty} T_y = 0, \quad \text{at } y = 0 \\ &u \to 0,\ u_p \to 0,\ v_p \to v,\ E \to 0,\ T \to T_\infty,\ C \to C_\infty,\ T_p \to T_\infty,\ C_p \to C_\infty. \quad \text{as } y \to \infty \end{aligned} \tag{10}$$

The non-dimensional form of the above-stated system phases may be obtained by introducing the subsequent transformations:

$$\begin{aligned} &u = bxF',\quad u_p = bxF'_p,\quad v_p = -\sqrt{\nu b}F_p,\quad v = -\sqrt{\nu b}F,\quad E = bx\sqrt{\frac{b}{\nu}}g(\eta), \\ &\theta_p = \frac{T_p - T_\infty}{T_f - T_\infty},\quad \theta = \frac{T - T_\infty}{T_f - T_\infty}\quad \phi = \frac{C - C_\infty}{C_w - C_\infty},\quad \phi_p = \frac{C_p - C_\infty}{C_w - C_\infty}\quad \eta = \sqrt{\frac{b}{\nu}}y \end{aligned} \tag{11}$$

Using Eq. (11) Eqs. (2)–(10) become:

$$F''' + FF' - F'^2 - MF' + Bg' + D_p\alpha_d\left(F'_p - F'\right) = 0 \tag{12}$$

$$\lambda g'' - \frac{\lambda}{G^*}(2g + F'') + Fg' - f'g = 0 \tag{13}$$

$$\theta'' - \Pr\gamma\left(FF'\theta' + F^2\theta''\right) + \Pr F\theta' M + D_p\alpha_d\left(\theta_p - \theta\right) + Q\theta + N_b\theta'\phi' + N_t\theta'^2 = 0, \tag{14}$$

$$\phi'' + ScF\phi' + \frac{N_t}{N_b}\theta'' - K_c\phi + Sc\beta_c l\left(\phi_p - \phi\right) = 0, \tag{15}$$

$$F_pF_p'' + \alpha_d\left(f' - F_p'\right) = 0. \tag{16}$$

$$F_p\theta_p' + \frac{1}{\Gamma\,\Pr}\alpha_d\left(\theta - \theta_p\right) = 0. \tag{17}$$

$$F_p\phi_p' + \beta_c l\left(\phi_p - \phi\right) = 0 \tag{18}$$

$$\begin{aligned} &F'(0) = 1 + \delta F'', \quad g(0) = -n_1F'', \quad \theta'(0) = -B_1(1 - \theta(0)), \quad N_b\phi'(0) + N_t\theta'(0) = 0, \\ &F'(\infty) = 1, \quad F_p = F, \quad \theta(\infty) = 0, \quad \theta_p(\infty) = 0, \quad \phi(\infty) = 0, \quad \phi_p(\infty) = 0. \end{aligned} \tag{19}$$

The quantities defined above are given by:

$$\begin{aligned} &\Pr = \frac{\upsilon}{\alpha}, \ G^* = \frac{\varepsilon b}{k^*\nu}, \quad \lambda = \frac{\varepsilon}{\rho_j\nu}, \quad \gamma = \lambda_1 b, M = \frac{\sigma B_0^2}{\rho b}, D_p = \frac{\rho_p}{\rho}, \quad \alpha_d = \frac{1}{\tau_m b}, \\ &N_b = \frac{\tau D_B C_\infty}{\nu}, \ N_t = \frac{\tau D_T \Delta T}{T_\infty \nu}, \ Sc = \frac{\upsilon}{D_B}, \ \Gamma = \frac{c_s}{c_p}, \ \delta = \alpha * \sqrt{\frac{b}{\nu}}, \ \beta_c = \frac{1}{\tau_c}, \\ &l = \frac{m\rho_p}{\rho}, \ B_1 = \frac{h_s}{k}\sqrt{\frac{b}{\nu}}, \quad Q = \frac{Q_0}{\rho c_p b}, K_c = \frac{K_r}{b}. \end{aligned} \tag{20}$$

Drag force coefficient in (C_F) and Sherwood number (Sh_x),are given by:

$$C_F = \frac{\tau_w}{\rho u_\infty^2}, \ Sh_x = \left.\frac{xq_n}{D_n(C_w - C_\infty)}\right|_{y=0}. \tag{21}$$

where

$$\tau_w = \mu\, u_y\big|_{y=0}, \quad q_n = -D_B C_y\big|_{y=0}, \tag{22}$$

The dimensionless forms of the aforementioned physical quantities are stated as under:

$$\sqrt{\mathrm{Re}_x}C_F = F''(0) \ Sh\sqrt{\mathrm{Re}_x} = -\phi'(0). \tag{23}$$

Numerical solution

The numerical methodology of MATLAB software bvp4c is implemented to evaluate the transformed coupled non-linear ordinary differential equations. The method bvp4c method possesses the following characteristics:

1. It is simple to use and has a quick convergence rate.
2. It has a reduced computing cost and, in comparison to other analytical techniques, a higher degree of accuracy.
3. For some problems, the shooting technique is unhelpful because it is sometimes very sensitive to early guesses and bvp4c, on the other hand, uses a collocation method that is more reliable than shooting.

With a mesh size, $h = 0.1$, the bvp4c method is used for ameliorate approximations (Fig. 2). The technique is authentic if the auxiliary conditions are fulfilled with a precision of 10^{-6}.

First of all, new variables are introduced as:

$$\begin{aligned} &y_1 = F, y_2 = F', y_3 = F'', yy_1 = F''', y_4 = F_p, y_5 = F_p', yy_2 = F_p'', y_6 = g, y_7 = g', yy_3 = g'', y_8 = \theta, \\ &y_9 = \theta', yy_4 = \theta'', y_{10} = \theta_p, yy_5 = \theta_p, y_{11} = \phi, y_{12} = \phi', yy_6 = \phi'', y_{13} = \phi_p, yy_7 = \phi_p', \end{aligned} \tag{24}$$

The following equations can be obtained using the above equations in the MATLAB bvp4c technique:

$$yy_1 = -y_1y_2 + y_2^2 + My_2 - By_7 - D_p\alpha_d\left(y_5 - y_2\right), \tag{25}$$

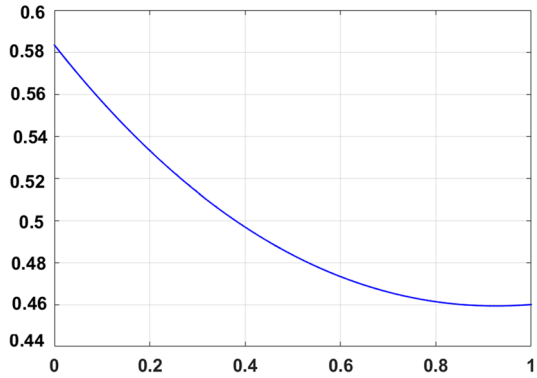

Figure 2. Mesh model.

$$yy_2 = \frac{-\alpha_d\left(y_2 - y_5\right)}{y_4}, \tag{26}$$

$$yy_3 = \left(\frac{\frac{\lambda}{G*}\left(2y_6 + y_3\right) - y_2y_7 + y_2y_6}{\lambda}\right), \tag{27}$$

$$yy_4 = \left(\frac{\left(\Pr\gamma\left(y_1y_2y_9\right)\right) - \Pr My_1y_9 + y_2^2 - D_p\alpha_d\left(y_{10} - y_8\right), -Qy_8 - N_by_9y_{12} - N_ty_9^2}{1 + \Pr\gamma y_1^2}\right), \tag{28}$$

$$yy_5 = \frac{\left(\frac{-1}{\Gamma\,\Pr}\alpha_d\left(y_8 - y_{10}\right)\right)}{y_4}, \tag{29}$$

$$yy_6 = -Scy_1y_{12} - \frac{N_t}{N_b}yy_4 + K_cy_{11} + Scl\beta_c\left(y_{13} - y_{11}\right), \tag{30}$$

$$yy_7 = \frac{l\beta_c\left(y_{13} - y_{11}\right)}{y_4}, \tag{31}$$

with the transmuted boundary conditions

$$\begin{aligned} &y_1(0) - 1 - \delta y_3(0), y_6(0) + ny_3(0), y_9(0) + B_1\left(1 - y_8(0)\right), N_by_{12}(0) + N_ty_9(0), \\ &y_2(\infty) - 1, y_4(\infty) - y_1(\infty), y_8(\infty), y_{10}(\infty), y_{11}(\infty), y_{13}(\infty), \end{aligned} \tag{32}$$

The flow chart (Fig. 3) of the implemented numerical scheme is appended as under:

Outcomes with discussion

This segment (Figs. 4, 5, 6, 7, 8, 9, 10, 11, 12, 13, 14, 15, 16, 17, 18) is developed to assess the evident attributes of the leading emergent parameters on the related profiles. Figures 4 and 5 depict that the velocity and temperature of dust particles surge as the fluid-particle interaction parameter α_d upsurges. This behavior can be caused by the fact that when the interaction between fluid and particles is high and the particle phase has thermal conductivity hegemony, the particle phase declines the liquid velocity till it reaches the same liquid velocity. This results in a fall in the fluid velocity and an upsurge in the velocity of dust particles. Figure 6 illustrates the influence of dust particle mass concentration (D_p) in the velocity field for the dust phase. It is observed that by growing D_p, the skin friction rises which causes difficulty in the movement of the nanofluid. Thus, $F_p'(\eta)$ declines. Figures 7 and 8 show the dimensionless velocity and thermal profiles in both dust and liquid phases for various estimations of the magnetic parameter (M). With increasing estimations of M, it is clear that the dimensionless velocities (F' and F_p') shrink, while the dimensionless temperatures (θ and θ_P) expand respectively. Physically, substantial Lorentz force initiates resistance in the liquid motion and the fluid develops more viscous that's why the velocity profile lowers. It is noted that for increasing values of M, the magnetic field has a thickening outcome on the thermal boundary layer which gives escalation to temperature. Figure 9 shows the velocity profile in both dust and liquid phases for distinct values of the coupling constant parameter (B). It is evident from this graph that both velocities (dust and liquid) are declining under the influence of B. The effect of the velocity slip parameter (δ) on the velocity profile is demonstrated in Fig. 10. The boundary layer thickness and velocity are found to drop as the δ is increased. When δ increases, some of the stretching velocity is shifted to the liquid. As a consequence, the velocity profile reduces. The sway of the thermal convection parameter (γ) on the fluid temperature is exhibited

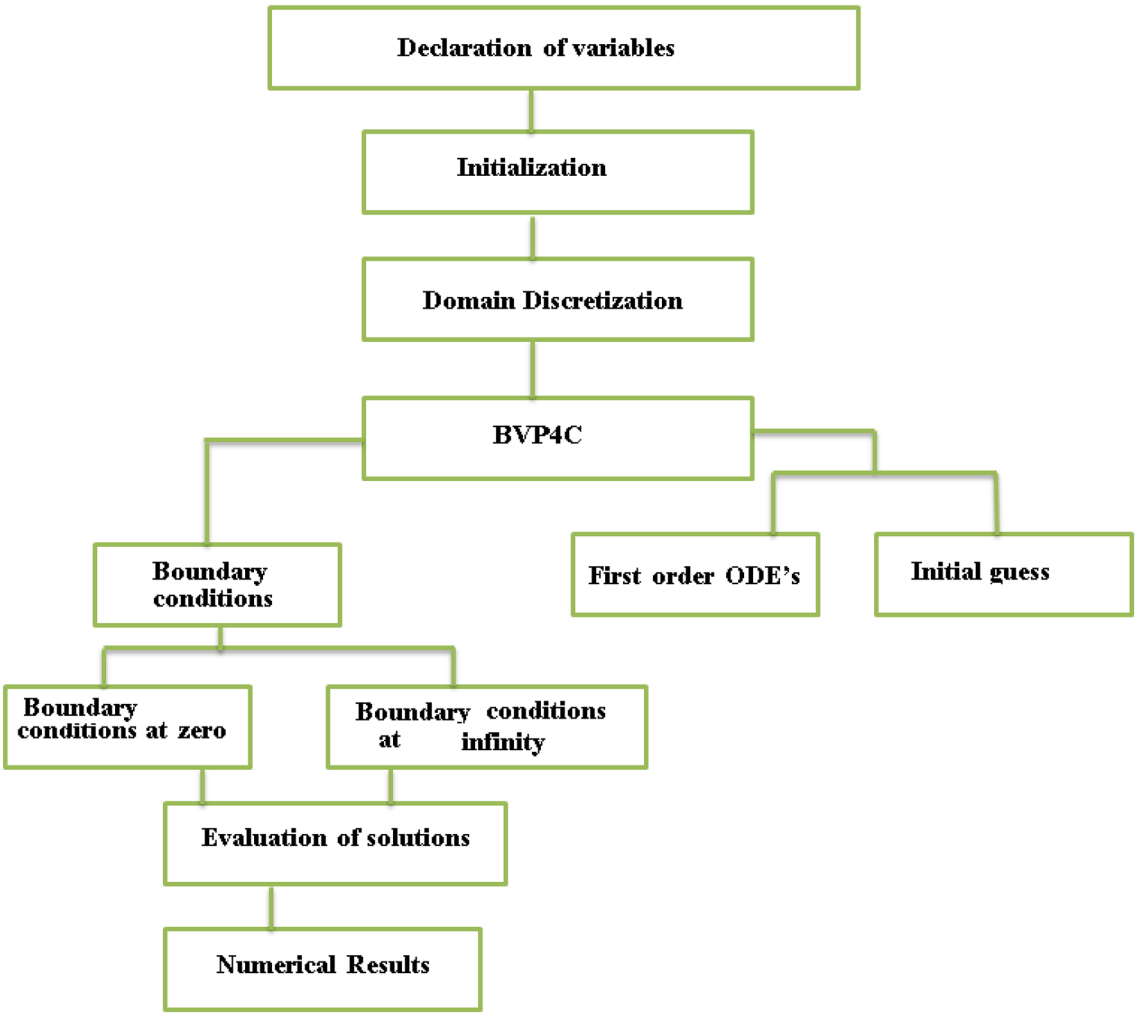

Figure 3. Flow chart of the numerical scheme.

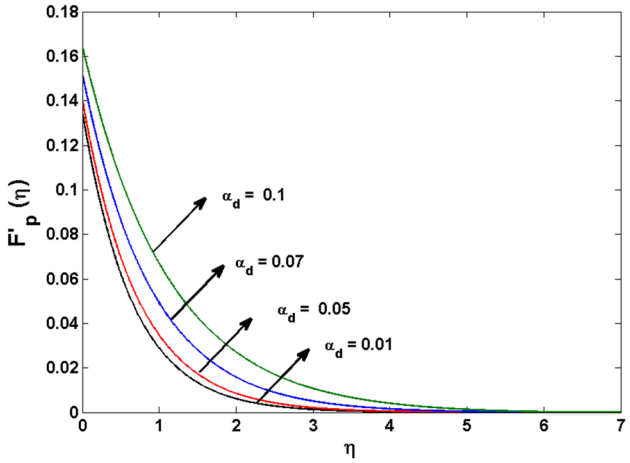

Figure 4. $F_p'(\zeta)$ for various estimates of α_d.

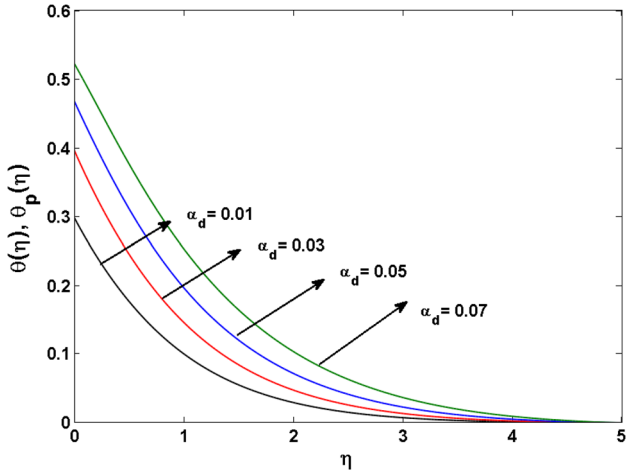

Figure 5. $\theta_p'(\zeta)$ for various estimates of α_d.

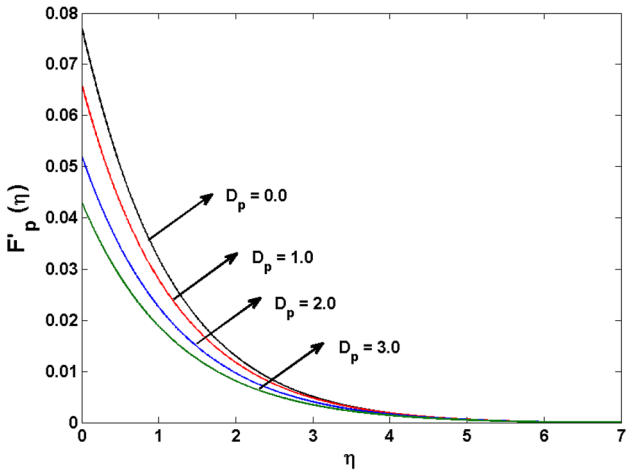

Figure 6. $F_p'(\zeta)$ for various estimates of D_p.

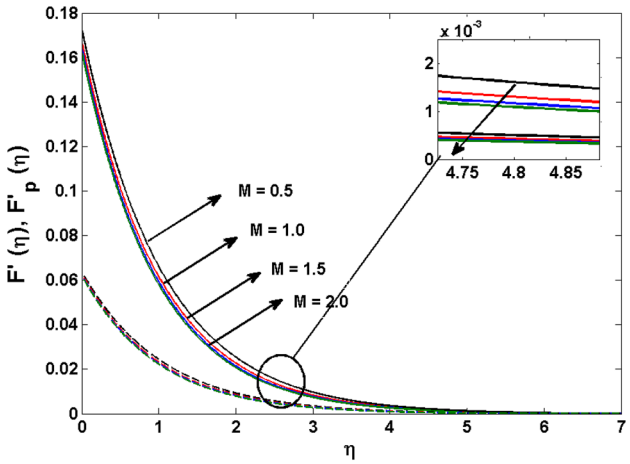

Figure 7. $F'(\eta)$ and $F_p'(\eta)$ for various estimates of M.

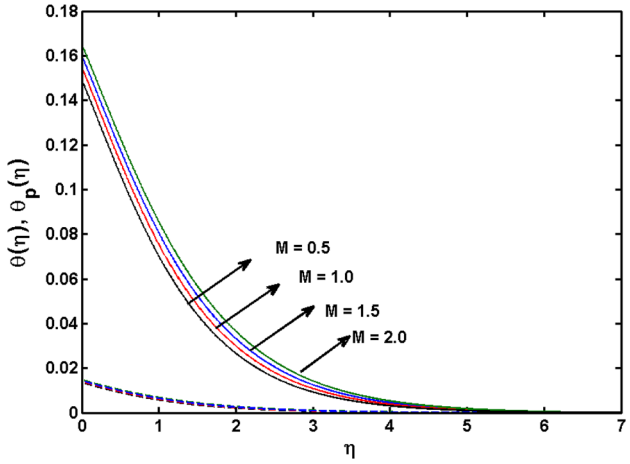

Figure 8. $\theta(\eta)$ and $\theta_p(\eta)$ for various estimates of M.

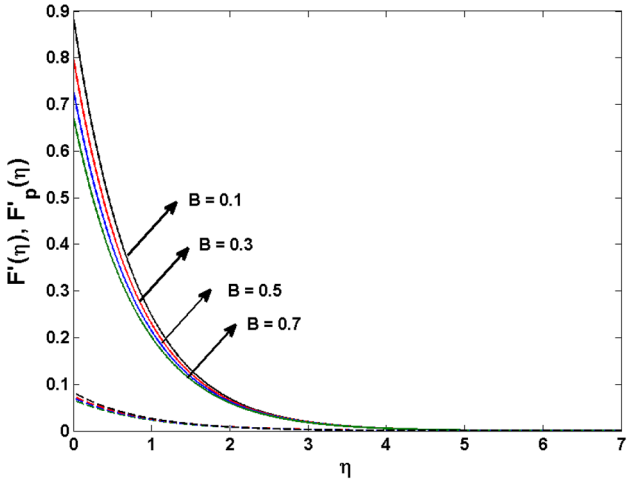

Figure 9. $F'(\eta)$ and $F'_p(\eta)$ for various B.

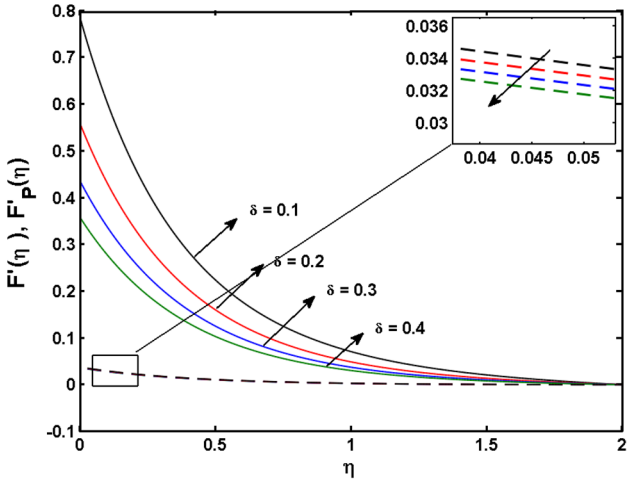

Figure 10. $F'(\eta)$ and $F'_p(\eta)$ for various estimates of δ.

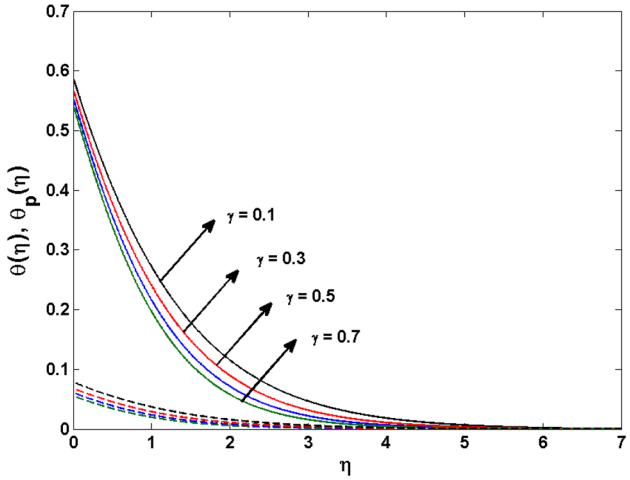

Figure 11. $\theta(\eta)$ and $\theta_p(\eta)$ for various estimates of γ.

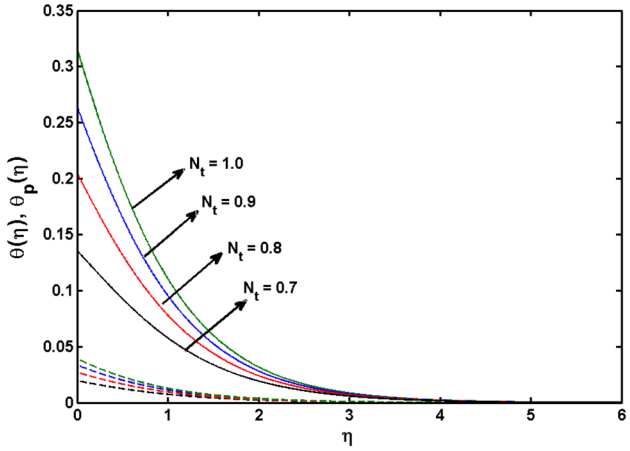

Figure 12. $\theta(\eta)$ and $\theta_p(\eta)$ for various estimates of N_t.

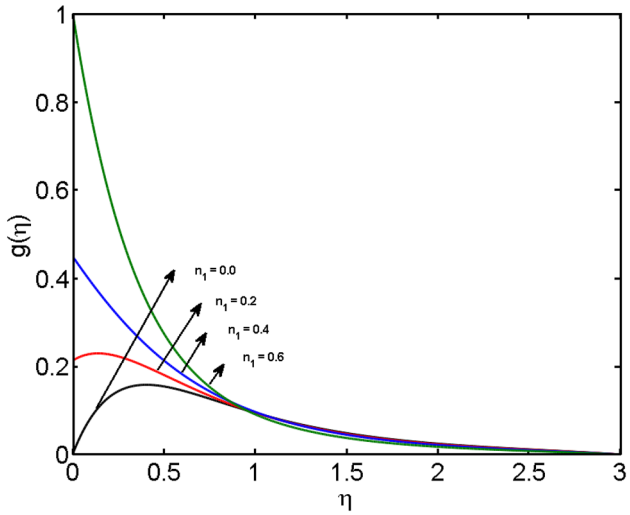

Figure 13. $g(\eta)$ for various estimates of n_1.

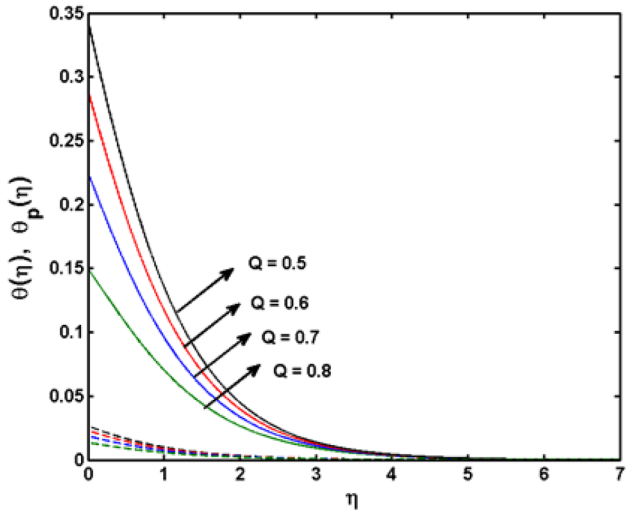

Figure 14. $\theta(\eta)$ and $\theta_p(\eta)$ for various estimates of Q.

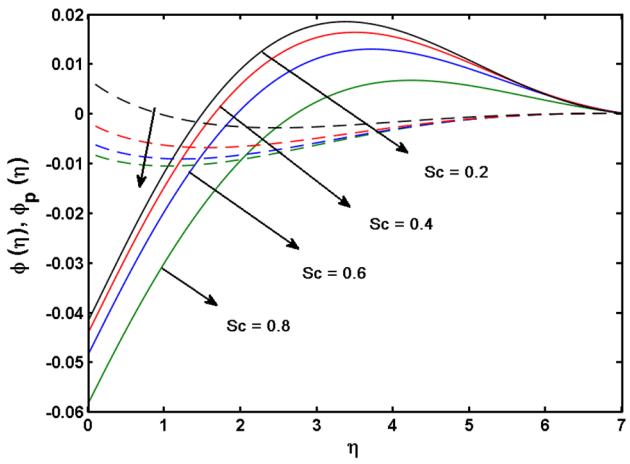

Figure 15. $\phi(\eta)$ for various estimates of Sc.

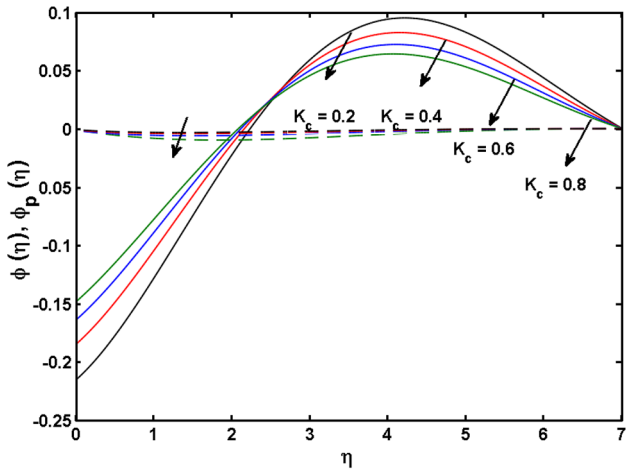

Figure 16. $\phi(\eta)$ for various estimates of K_c.

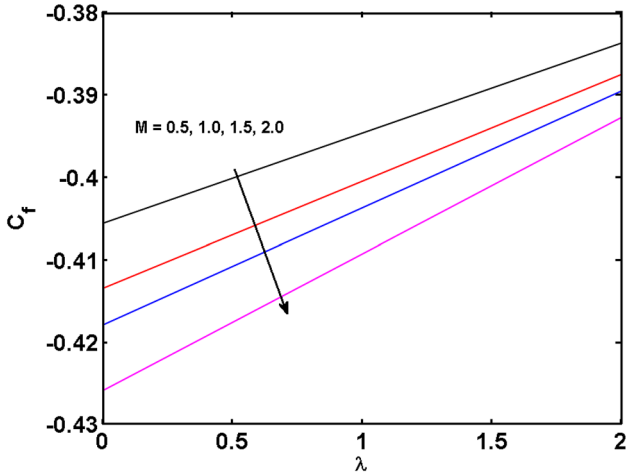

Figure 17. C_F for various of estimates of M and λ.

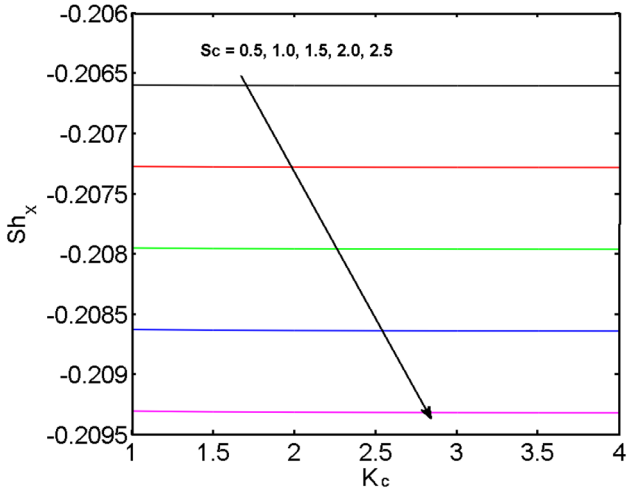

Figure 18. Sh_x for various estimates of K_c and Sc.

in Fig. 11. It is illustrated that both liquid and dust phases thickness of the thermal boundary layer are lessened for mounting estimates of γ. Greater values of relaxation times result in non-conductive behavior of the material which is liable for decay in the thermal profile. Figure 12 indicates the effect of the thermophoresis parameter (N_t) on the thermal profile. The higher temperature is seen for large estimations of N_t. This is due to an increase in the number of nanoparticles of fluid approaching the hot surface, causing the temperature profile to rise. In Fig. 13, the estimation of angular velocity (n_1) increases for higher values of n. For $n_1 = 0$ leads to $g = 0$ which indicated that there is no-spin condition according to the boundary condition at the wall, $g(0) = -n_1 F''$, this means that the microelements in the concentrated particle flow near the wall surface are unable to rotate. For $n_1 = 0.5$ when $g \neq 0$, it indicates that the anti-symmetric component of the stress tensor disappears and is replaced by a weak concentration. The particle spin must be comparable to the fluid velocity at the wall in fine particle movements. The impact of sink/source parameter (Q) versus thermal profile is displayed in Fig. 14. It is illustrated that the thermal profile reduces for greater estimation of Q. Figure 15 is outlined to study the impact of Schmidt number (Sc) on the concentration profile. For greater valuations of Sc feeble concentration is noticed. Greater values of Sc result in smaller Brownian diffusivity. This weak Brownian diffusivity will lower the concentration field. In Fig. 16, the impact of chemical reaction K_c on concentration field is addressed. Here, one can observe that the concentration field decreases for large estimations of K_c . It is perceived that greater values of K_c result in decay in the concentration profile. Figure 17 illustrated the influence on the surface Drag force coefficient C_F for M and λ. It is noticed that the C_F decreases versus growing values of M. The influence of Sh_x for K_c and Sc is revealed in Fig. 18. It is examined that Sh_x decline for greater Sc. Table 2 depict the comparison of magnetic parameter M with Akbar et al.[34] and Gireesha et al.[35]. The outcomes are found in anoutstanding agreement.

M	[15]	[16]	Present
01	− 1.41421	− 1.41421	− 1.41420
05	− 2.44948	− 2.44949	− 2.44949
10	− 3.31662	− 3.31662	− 3.31664
50	− 7.14142	− 7.14143	− 7.14140
500	− 22.3830	− 22.38302	− 22.3831
1000	− 31.6386	− 31.63858	− 31.6359

Table 2. Comparison values of Skin friction co-efficient ($B = 0$).

Final remarks

In this research, we have examined the role of modified Fourier law in the flow of an MHD Micropolar nanoliquid flow with dust particles over a stretched surface. The distinctiveness of the presented model is boosted with additional impacts of the chemical reaction and the heat source/sink with slip, convective and zero mass flux conditions at the boundary. The erected model is handled numerically with the bvp4c function of MATLAB software. The results are obtained graphically for the associated profiles versus respective parameters and discussed logically. A comparison is also made with a published paper to ascertain the validity of the presented model. The answers to the above raised questions with other salient highlights are appended as:

- The velocity and temperature of dust particles rise as the fluid-particle interaction parameter increases.
- For positive values of magnetic parameter, dimensionless velocity decreases while temperature profile increases in both dust and liquid phases.
- In both dust and liquid phases, the thermal boundary layer thickness is lessened for growing estimates of thermal relaxation time.
- The thickness of the boundary layer and velocity was found to decline as the velocity slip parameter is heightened.
- The mass transfer rate reduces by escalating the Schmidt number and chemical reaction parameter.
- The fluid and dust phases are enhanced for gradual escalated estimations of the heat source/sink parameter.

Received: 20 June 2021; Accepted: 6 September 2021
Published online: 30 September 2021

References

1. Hady, F. M., Mahdy, A., Mohamed, R. A. & Zaid, O. A. A. Modeling non-Darcy natural convection flow of a micropolar dusty fluid with convective boundary condition. *Int. J. Aerosp. Mech. Eng.* **14**(2), 41–47 (2020).
2. Begum, N. *et al.* Numerical solutions for gyrotactic bioconvection of dusty nanofluid along a vertical isothermal surface. *Int. J. Heat Mass Transf.* **113**, 229–236 (2017).
3. Nabwey, H. A. & Mahdy, A. Numerical approach of Micropolar dust-particles natural convection fluid flow due to a permeable cone with nonlinear temperature. *Alex. Eng. J.* **60**(1), 1739–1749 (2021).
4. Nabwey, H. A. & Mahdy, A. Transient flow of Micropolar dusty hybrid nanofluid loaded with Fe_3O_4–Ag nanoparticles through a porous stretching sheet. *Results Phys.* **21**, 103777 (2021).
5. Pattnaik, P. K., Mishra, S. R. & Sharma, R. P. Numerical simulation for flow through conducting metal and metallic oxide nanofluids. *J. Nanofluids* **9**(4), 354–361 (2020).
6. Jena, S., Mishra, S. R. & Pattnaik, P. K. Development in the heat transfer properties of nanofluid due to the interaction of inclined magnetic field and non-uniform heat source. *J. Nanofluids* **9**(3), 143–151 (2020).
7. Jena, S., Mishra, S. R., Pattnaik, P. K. & Sharma, R. P. The nanofluid flow between parallel plates and heat transfer in presence of chemical reaction and porous matrix. *Lat. Am. Appl. Res. Int. J.* **50**(4), 283–289 (2020).
8. Mohanty, B., Jena, S., & PK, P. Mhd Nanofluid Flow Over Stretching/Shrinking Surface in Presence of Heat Radiation Using Numerical Method. International Journal on Emerging Technologies **10**(2b), 119–125 (2019)
9. Rashidi, M. M. *et al.* Semi-analytical solution of two-dimensional viscous flow through expanding/contracting gaps with permeable walls. *Math. Comput. Appl.* **26**(2), 41 (2021).
10. Pattnaik, P. K. & Biswal, T. Analytical solution of MHD free convective flow through porous media with time dependent temperature and concentration. *Walailak J. Sci. Technol. WJST* **12**(9), 749–762 (2015).
11. Mishra, S. R., Pattnaik, P. K., Bhatti, M. M. & Abbas, T. Analysis of heat and mass transfer with MHD and chemical reaction effects on viscoelastic fluid over a stretching sheet. *Indian J. Phys.* **91**(10), 1219–1227 (2017).
12. Pattnaik, P. K., Mishra, S. R., Barik, A. K. & Mishra, A. K. Influence of chemical reaction on magnetohydrodynamic flow over an exponential stretching sheet: a numerical study. *Int. J. Fluid Mech. Res.* **47**(3), 217–228 (2020).
13. Pattnaik, P. K., Mishra, S. R., Mahanthesh, B., Gireesha, B. J. & Rahimi-Gorji, M. Heat transport of nano-micropolar fluid with an exponential heat source on a convectively heated elongated plate using numerical computation. *Multidiscip. Model. Mater. Struct.* **16**, 1295–1312 (2020).
14. Pattnaik, P. K., Mishra, S. & Bhatti, M. M. Duan-rach approach to study Al_2O_3–ethylene glycol $C_2H_6O_2$ nanofluid flow based upon KKL model. *Inventions* **5**(3), 45 (2020).
15. Barik, A. K., Mishra, S. K., Mishra, S. R. & Pattnaik, P. K. Multiple slip effects on MHD nanofluid flow over an inclined, radiative, and chemically reacting stretching sheet by means of FDM. *Heat Transf. Asian Res.* **49**(1), 477–501 (2020).
16. Mishra, S. R., Pattnaik, P. K. & Dash, G. C. Effect of heat source and double stratification on MHD free convection in a micropolar fluid. *Alex. Eng. J.* **54**(3), 681–689 (2015).
17. Mishra, S., Mahanthesh, B., Mackolil, J. & Pattnaik, P. K. Nonlinear radiation and cross-diffusion effects on the micropolar nanoliquid flow past a stretching sheet with an exponential heat source. *Heat Transf.* **50**(4), 3530–3546 (2021).

18. Ali, B., Pattnaik, P. K., Naqvi, R. A., Waqas, H. & Hussain, S. Brownian motion and thermophoresis effects on bioconvection of rotating Maxwell nanofluid over a Riga plate with Arrhenius activation energy and Cattaneo-Christov heat flux theory. *Therm. Sci. Eng. Prog.* **23**, 100863 (2021).
19. Khan, T., & Chaudhary, H. An investigation on parameter identification method of controlling chaos in generalized Lotka–Volterra systems via hybrid projective difference combination synchronization technique. In *Advances in Mechanical Engineering* 547–558. (Springer, Singapore, 2021).
20. Krishnamurthy, M. R., Prasannakumara, B. C., Gorla, R. S. R. & Gireesha, B. J. Non-linear thermal radiation and slip effect on boundary layer flow and heat transfer of suspended nanoparticles over a stretching sheet embedded in porous medium with convective boundary conditions. *J. Nanofluids* **5**(4), 522–530 (2016).
21. Radhika, M., Punith Gowda, R. J., Naveenkumar, R. & Prasannakumara, B. C. Heat transfer in dusty fluid with suspended hybrid nanoparticles over a melting surface. *Heat Transf.* **50**(3), 2150–2167 (2021).
22. Kumar, K. G. *et al.* Significance of Arrhenius activation energy in flow and heat transfer of tangent hyperbolic fluid with zero mass flux condition. *Microsyst. Technol.* **26**(8), 2517–2526 (2020).
23. Madhukesh, J. K. *et al.* Numerical simulation of AA7072-AA7075/water-based hybrid nanofluid flow over a curved stretching sheet with Newtonian heating: A non-Fourier heat flux model approach. *J. Mol. Liq.* **335**, 116103 (2021).
24. Molla, M. M., Hossain, M. A. & Paul, M. C. Natural convection flow from an isothermal horizontal circular cylinder in presence of heat generation. *Int. J. Eng. Sci.* **44**, 949–958 (2006).
25. Hassan, M., Mohyud-Din, S. T. & Ramzan, M. Study of heat transfer and entropy generation in ferrofluid under low oscillating magnetic field. *Indian J. Phys.* **93**(6), 749–758 (2019).
26. Molla, M. M., Hossain, M. A. & Taher, M. A. Magnetohydrodynamic natural convection flow on a sphere with uniform heat flux in presence of heat generation. *Acta Mech.* **186**(1–4), 75 (2006).
27. Baron Fourier, J. B. J. (1822). Théorie analytique de la chaleur. F. Didot.
28. Cattaneo, C. Sulla conduzione del calore. *Atti Sem. Mat. Fis. Univ. Modena* **3**, 83–101 (1948).
29. Christov, C. I. On frame indifferent formulation of the Maxwell-Cattaneo model of finite-speed heat conduction. *Mech. Res. Commun.* **36**(4), 481–486 (2009).
30. Kumar, R. V., Gowda, R. P., Kumar, R. N., Radhika, M. & Prasannakumara, B. C. Two-phase flow of dusty fluid with suspended hybrid nanoparticles over a stretching cylinder with modified Fourier heat flux. *SN Appl. Sci.* **3**(3), 1–9 (2021).
31. Ramzan, M., Bilal, M. & Chung, J. D. MHD stagnation point Cattaneo–Christov heat flux in Williamson fluid flow with homogeneous–heterogeneous reactions and convective boundary condition—A numerical approach. *J. Mol. Liq.* **225**, 856–862 (2017).
32. Prasad, K. V., Vaidya, H., Vajravelu, K. & Ramanjini, V. Analytical study of Cattaneo–Christov heat flux model for Williamson-nanofluid flow over a slender elastic sheet with variable thickness. *J. Nanofluids* **7**(3), 583–594 (2018).
33. Ullah, K. S., Ali, N., Hayat, T. & Abbas, Z. Heat transfer analysis based on Cattaneo–Christov heat flux model and convective boundary conditions for flow over an oscillatory stretching surface. *Therm. Sci.* **23**(2), 443–455 (2019).
34. Akbar, N. S., Nadeem, S., Haq, R. U. & Khan, Z. H. Numerical solutions of Magnetohydrodynamic boundary layer flow of tangent hyperbolic fluid towards a stretching sheet. *Indian J. Phys.* **87**(11), 1121–1124 (2013).
35. Gireesha, B. J., Shankaralingappa, B. M., Prasannakumar, B. C. & Nagaraja, B. MHD flow and melting heat transfer of dusty Casson fluid over a stretching sheet with Cattaneo–Christov heat flux model. *Int. J. Ambient Energy* https://doi.org/10.1080/01430750.2020.1785938 (2020).
36. Souayeh, B. *et al.* Slip flow and radiative heat transfer behavior of Titanium alloy and ferromagnetic nanoparticles along with suspension of dusty fluid. *J. Mol. Liq.* **290**, 111223 (2019).
37. Anuar, N. S., Bachok, N. & Pop, I. Numerical computation of dusty hybrid nanofluid flow and heat transfer over a deformable sheet with slip effect. *Mathematics* **9**(6), 643 (2021).

Acknowledgements

The authors extend their appreciation to the Deanship of Scientific Research at King Khalid University, Abha 61413, Saudi Arabia for funding this work through research groups program under Grant Number RGP-1-36-42.

Author contributions

M.R. supervised and conceived the idea; H.G. wrote the manuscript; M.Y.M. did work on the graphical illustrations. D.B. and K.S.N. helped in revising the manuscript and arrangement of funds.

Competing interests

The authors declare no competing interests.

Additional information

Correspondence and requests for materials should be addressed to M.R.

Reprints and permissions information is available at www.nature.com/reprints.

Publisher's note Springer Nature remains neutral with regard to jurisdictional claims in published maps and institutional affiliations.